Florida International University

FIU Digital Commons

1-1-2022

Bandwidth enhancement of antennas designed by band-pass filter synthesis due to frequency pulling techniques

Anastasios G. Koutinos
Democritus University of Thrace

George A. Kyriacou
Democritus University of Thrace

John L. Volakis
Florida International University

Michael T. Chryssomallis
Democritus University of Thrace

Follow this and additional works at: https://digitalcommons.fiu.edu/ece_fac

IET Microwaves, Antennas & Propagation

ORIGINAL RESEARCH PAPER

Bandwidth enhancement of antennas designed by band-pass filter synthesis due to frequency pulling techniques

Anastasios G. Koutinos[1] | **George A. Kyriacou**[1] | **John L. Volakis**[2] |
Michael T. Chryssomallis[1]

[1]Electrical and Computer Engineering Department, Democritus University of Thrace, Xanthi, Greece

[2]College of Engineering and Computing, Florida International University, Miami, Florida, USA

Correspondence

Michael T. Chryssomallis, Department of Electrical and Computer Engineering, Democritus University of Thrace, Xanthi 67100, Greece.
Email: mchrysso@ee.duth.gr

Funding information

Hellenic Foundation for Research and Innovation; General Secretariat for Research and Technology, Grant/Award Number: 2047

Abstract

A novel antenna design technique is proposed, which offers bandwidth enhancement up to the limits defined by element radiation efficiency. The employed technique is referred as frequency pulling (FP) as it mimics the 'insertion loss design methodology of band-pass filters'. This is essentially a wideband matching approach pushing the antenna efficiency to the limits set up by radiation efficiency. There are three options towards this trend: (i) first to enhance a single element bandwidth (compact element) exploiting its possibly multiple symmetrical feeding points as distinct resonator ports, (ii) frequency pulled array as to design a small antenna array (less than about 10 elements) where each element acts as a resonator and (iii) second order frequency-pulled array as to build a small array using compact elements of category (i). Similar to the band-pass filter design, all antennas or distinct-port circuits resonate at the same resonant frequency when isolated, cascading two or more of them; FP yields to multiple-overlapping successive resonances in their overall response. Although the proposed technique is general within this first effort, it is applied to simple patch antenna elements exhibiting multiple symmetrical feeding points, namely two—for rectangular, four—for square and five—for pentagonal. The third option is applied to an array of three compact 4-feeding point square elements offering triple bandwidth with respect to the already wideband single element. However, this is achieved at the expense of a significant beam squint. Thus, in general, these wideband compact elements should be used within a classical array design. Further bandwidth enhancement using FP to antenna elements with inherent multiple resonances as patches with slots or truncated edges constitutes our next task. Their inherent wider bandwidth in radiation efficiency is expected to allow multiply higher bandwidths when exploited with our FP technique.

KEYWORDS

antenna arrays, antenna feeds, band-pass filters, broadband antennas, impedance matching

1 | INTRODUCTION

With the adaptation of 5G communications, there is a need for bandwidth increase without significant redesign of existing antennas. Several antenna miniaturisation techniques and bandwidth enhancements of classical antennas have been presented in the recent past [1–3]. Specifically, bandwidth enhancement in patch antennas can be achieved through the use of various modifications such as the use of slots [4–6], lower permittivity dielectric [7] or a slight increase in height [8, 9]. Another way to increase bandwidth is by modifying the feeding of the antenna. For example the placement of the L-shaped feeding probe, which acts as an equivalent resonant circuit between the patch and the feed and alters the quality factor of the structure, further enhances the bandwidth and reduces the size of the antenna [10]. There are also different feeding methods, described in Refs.

[9, 11, 12]. The common concept in the aforementioned methods refers to the establishment of multiple resonances in the radiating structure, that is, simultaneous excitation of two or three resonating modes in the patch antenna or the combination of the resonating patch and resonating slot. These resonances are separated but close enough for the overall response to be a unified extended frequency band. The question is whether the operating bandwidth of each one of them (operating at a single or multiple resonances) could be extended by manipulating their feeding structure. It is common knowledge that the radiation efficiency of these antennas has a much wider bandwidth than their antenna efficiency. A solution towards this direction stems from the 'band-pass filter (BPF) synthesis', where a number of high quality factor (narrowband) stages resonating at the same central frequency are combined to offer a wide pass band filter. The concept behind this synthesis is the 'frequency pulling (FP)', that is, when two of these resonators are cascaded, the circuit presents three overlapping resonances. Namely their common resonant frequency is pulled downwards and upwards, while the original common resonance is retained. Regarding this concept, we started modifying the feeding network of classical patch antennas observing an impressive bandwidth enhancement, just as predicted by FP in BPF synthesis [13–16]. Advantages offered by BPF but without any reference to FP were also exploited by other researchers [17, 18].

A filter synthesis was followed in Ref [17], but it was specifically applied to waveguide aperture antennas. A series of publications elaborate on the band-pass filter and antenna co-design, known as 'filtering antennas' or shortly 'filtennas', [19–26]. A common characteristic of these methodologies is their attempt to formulate the antenna feeding network as a band-pass filter, without any reference to matching the antenna efficiency to radiation efficiency. It is towards this direction that our present effort is elaborating but exploiting the antenna itself as a resonant stage. It seems that there are only two publications utilising the radiating elements as resonators in waveguide type antennas [18] and multiple coupled resonators [27]. However, it is to our knowledge herein for the first time that a systematic approach is presented for the design of antennas exploiting the FP of BPF synthesis.

Overall, in this study a novel general antenna design technique is presented that systematically exploits the 'FP' principle of band-pass filters for bandwidth enhancement while retaining minimal dimensions. The technique herein is applied in three stages: (i) Single ordinary patches with multiple symmetrical feeding points to yield compact wideband antennas, (ii) A small array of the travelling wave (TWA) type aiming at wideband operation rather than beamforming and (iii) Second order FP as a small frequency pulled antenna with compact antenna elements, pushing the bandwidth to its upper limits set by radiation efficiency. However, the quarter wave lines utilised as impedance inverters between successive elements to realise FP correspond to a $-90°$ ($-\pi/2$) phase shift causing beam steering (or a beam squint) by $kd\sin\theta_o = \pi/2$, which for the interelement distance $d = \lambda/2$ yields a beam squint by $\theta_o = 30°$. Thus, such arrays can be comprised of only a few elements (e.g. up to 4) and for applications where

wideband operation is important so that beam width remains wide and its beam maximum orientation is not critical. On the contrary, the obtained wideband compact elements can be utilised within classical antenna array design methodologies allowing ordinary beam shaping and beamforming within the bandwidth offered by these elements. Our plans to further enhance the bandwidth without any degradation refer to the utilisation of the above scheme for single elements with inherent multiple resonances such as square patches with truncated corners or with etched slots as well as aperture-coupled fed antennas. In any case, FP is expected to push the antenna efficiency close to the limits set by the element radiation efficiency.

The study is organised as follows: Section 2 describes the FP of band-pass filters and how ordinary stub resonators can be substituted by patch antennas. Design cases using the FP technique are presented in Section 3. The designed and demonstrated cases are: A TWA (case ii), a simple multi-feed patch (case i) and a multi-feed array antenna (case iii) as well as an array of three compact elements without second order FP. Section 4 concludes the work.

2 | DESCRIPTION OF DESIGN METHODOLOGY

2.1 | Design procedure outline

The design starts applying the synthesis process of a band-pass filter [28]. Using the insertion loss method and Chebyshev equal ripple response from a low-pass prototype, a BPF is constructed (Figure 1a,b). Thus, a structure of shunt-connected parallel resonators is created. As a next step, we replace the shunt resonators with appropriate stubs behaving in the same way. The resonant circuits can be replaced equivalently by quarter wavelength short-circuited or half wavelength open-circuited stubs, both of which behave as parallel resonant circuits (Figure 1c). Although there are alternative implementations, here we choose the microstrip technology. Thus, we use half wavelength open-circuited stubs, which as resonators are equivalent to patch antennas and are more likely able to radiate. By this way, the constructed BPF takes the form of a travelling wave array (Figure 1d). It is important to mention, as explained above, that the frequency-pulled antenna only aims at a wider operational bandwidth rather than beamforming, which is somehow sacrificed in this case by accepting of up to a 30° beam squint. The resistor load at the terminal is replaced by the resistors representing losses on each antenna element. Finally, by feeding a single antenna at different symmetrical feeding points, the structure produced (Figure 1e) is expected to have the same frequency response as that of the assumed BPF.

The constructed BPF operates with enhanced bandwidth and either in the form of a ladder-type circuit of series and parallel resonant circuits or at the final stage of a travelling wave array consisting of a series of patch antennas that can be used for the explanation of FP. The larger bandwidth is due to
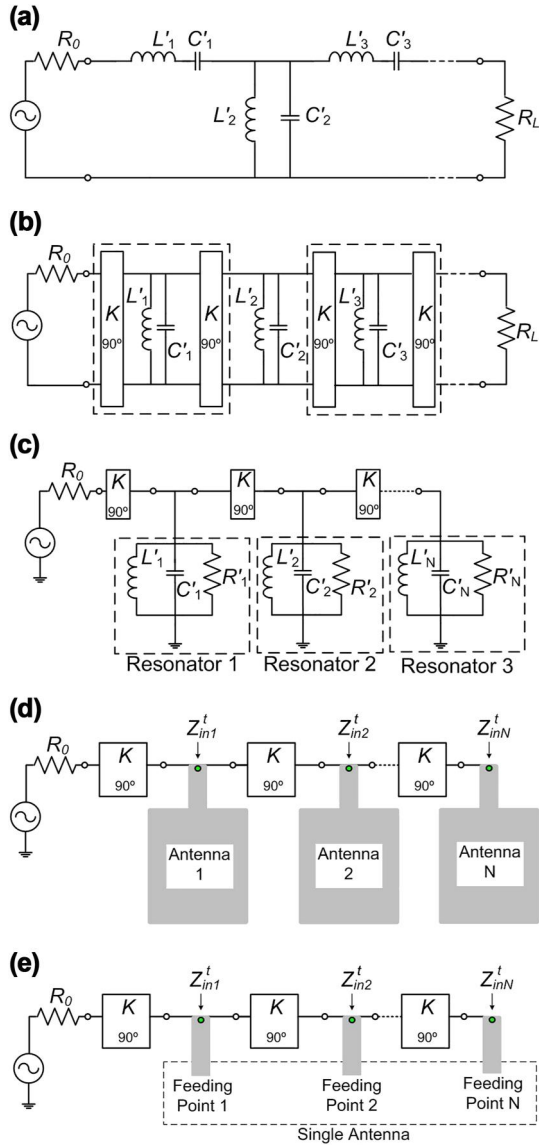
FIGURE 1 Basic steps in the design of a frequency pulled antenna: (a) band-pass filter design, (b) transformation of series resonators to parallel ones, (c) replacement of discrete elements resonators with open-circuited stubs, (d) replacement of stubs with patch antennas, and (e) replacement of antennas with symmetrical feeding points of a single antenna

the multiple successive resonances created by the FP occurring when resonant circuits are cascaded. Actually, FP generates new resonant frequencies, which are identical to the natural or eigenfrequencies of the coupled resonators. This is the same phenomenon as the one appearing in the filter theory. The cascaded circuits forming the BPF undergo a phase shift in much the same way as short and open stubs are used for wideband impedance matching. One has to keep in mind that these overlapping resonances occur at the structure input port while the antenna element (resonator) retains its modal-operating radiation characteristics. Thus, the employed FP affects—enhance the input—port matching to the feeding line, but it does not disturb the element radiation properties. Notably, a pair of shorted and open stubs is used to realise the

Marchand Balun. The latter has been recently used to develop wideband feeds for the tightly coupled dipole arrays [27].

2.2 | Analysis of design technique

In order to demonstrate the way FP leads to bandwidth extension, we use a second order BPF in its initial form as shown in Figure 2. The inclusion of ohmic resistances in series and parallel resonators ensures the equivalence of resonators to patch antennas with least radiation losses by giving meaning to the existence of their quality factor. It is well established that all isolated elements of a filter must resonate at the same frequency but with a different quality factor given as, $Q_{si} = \omega_0 L_i / R_i$ and $Q_{pi} = \omega_0 R_i C_i$ for the series and parallel resonator, respectively, where ω_0 is the resonant frequency [28].

FP in the sequence of series and parallel resonant circuits, resulting in additional resonances, ω_{r1} and ω_{r2}, below and above ω_0, respectively. Namely, the resonant frequency of the second resonator, as seen at the input of the BPF, is pulled by the precedent first resonator downwards and upwards by an equal amount $\Delta\omega$. To clarify this effect, the input impedance of the second order BPF of Figure 2 is examined for resonances and its transfer function is extracted. The input impedance of the circuit is given by

$$Z_{in} = \frac{(Z_1 + R_L) + Z_1 R_L Y_2}{1 + R_L Y_2} = \frac{1 + Z_1 Y_2 + Z_1/R_L}{1 + R_L Y_2} \quad (1)$$

where all parameters are denoted in Figure 2.

Taking the open-circuit resonances by letting $R_L \to \infty$, Equation (1) reduces to

$$Z_{in}^{oc} = Z_1 + 1/Y_2 = Z_1 + Z_2 \quad (2a)$$

Expecting a resonance shift from ω_o to $\omega_r = \omega_o \pm \Delta\omega_r$ and approximating Z_1 and Y_2 according to Ref. [28] as

$$Z_1 \approx R_1 + j2L_1\Delta\omega_r \quad (2b)$$

$$Y_2 \approx 1/R_2 + j2C_2\Delta\omega_r \quad (2c)$$

The new resonances at $\omega_o \pm \Delta\omega_r$ can be estimated by equating the phase of Z_{in} to zero. After some calculations we find that,

$$\Delta\omega_{r1,2} = \pm \frac{1}{2R_2 C_2} \sqrt{\frac{R_2^2 C_2}{L_1} - 1} \quad (3)$$

With the use of a circuit simulator, FP can be explained graphically from the results shown in Figure 3. In this figure, the amplitude and phase of Z_{in} of BPF of Figure 2 are drawn for the serial and parallel resonant circuits, each one alone and for the combination of them, that is, a series resonance cascaded by a parallel resonance. Resonance occurs at the zero
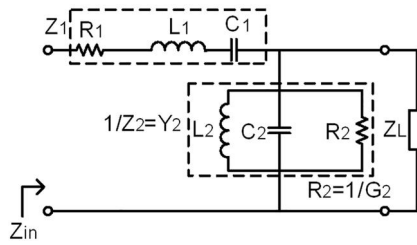
FIGURE 2 Equivalent ladder-type circuit of a second order band-pass filter. R_1, R_2 represent the ohmic losses of resonant circuits

phase; thus, the overall input impedance [Equation (2a)] has series resonances at $\mathrm{Im}(Z_{\mathrm{in}}^{\mathrm{oc}}) = 0$ or

$$\theta^{\mathrm{oc}} = 0 \leftrightarrow |Z_1|\sin\theta_1 = |Z_2|\sin\theta_2 \qquad (4)$$

This can be understood from Figure 3b, where at some frequency $\omega_{\mathrm{o}} + \Delta\omega_{\mathrm{r}}$, above ω_{o} resonance and the negative phase $-\Delta\varphi$ inserted by Z_1 is compensated by the positive phase shift $+\Delta\varphi$ introduced by Z_2. The opposite occurs at a lower frequency $\omega_{\mathrm{o}} - \Delta\omega_{\mathrm{r}}$. Hence, for the cascaded circuit of two resonators of Figure 2, the single resonance, originally existed at ω_{o}, occurs simultaneously at two new frequencies, $\omega_{\mathrm{o}} - \Delta\omega_{\mathrm{r}}$ and $\omega_{\mathrm{o}} + \Delta\omega_{\mathrm{r}}$. The original resonance at ω_{o}, is retained between the new ones but for different impedance as is shown in Figure 3a. It is important to observe that the two new resonances at $\omega_{\mathrm{o}} \pm \Delta\omega_{\mathrm{r}}$ have a lower quality factor and equivalently wider bandwidth than the resonance at ω_{o} as shown in Figure 3c.

For a more general investigation of FP, the voltage transfer function $H(j\omega)$ for BPFs of order 1, 2 and 3 are given in Table 1. For a band-pass response, $H(j\omega)$ should be maximised at resonance, which corresponds to setting the imaginary part of its denominator to zero.

The resulting resonant frequencies are also depicted in the same table, where for the resonators, only elements L and C are used. As expected, the two approaches yield the same resonant frequencies for the second order filter if we eliminate the ohmic resistances by letting $R_1 \rightarrow 0$ and $R_2 \rightarrow \infty$.

In Figure 4, we plot on a Smith chart, the impedance locus of the two resonators and their cascaded combination of BPF of Figure 2. As can be seen, the trajectories of the series and parallel resonators, when they are alone, intersect the x axis at ω_{o} moving from opposite directions. Their cascaded combination intersects the x axis two more times where these points correspond to the new resonances at $\omega_{\mathrm{o}} \pm \Delta\omega_{\mathrm{r}}$. It passes also from ω_{o}, which is between them and happens for higher impedance but can still be considered to contribute to a single enhanced bandwidth. In all three cases, the 3-dB bandwidth is defined by the constant $Q = X/R = 1$ trajectories.

As already described, the series resonant circuits are transformed into equivalent parallel ones by using quarter wavelength transformers as impedance inverters. In this way, a structure of only shunt or parallel resonators is constructed. The next step is to replace the shunt resonators of lumped elements with distributed form resonators using appropriate stubs. They can be replaced equivalently by quarter wavelength

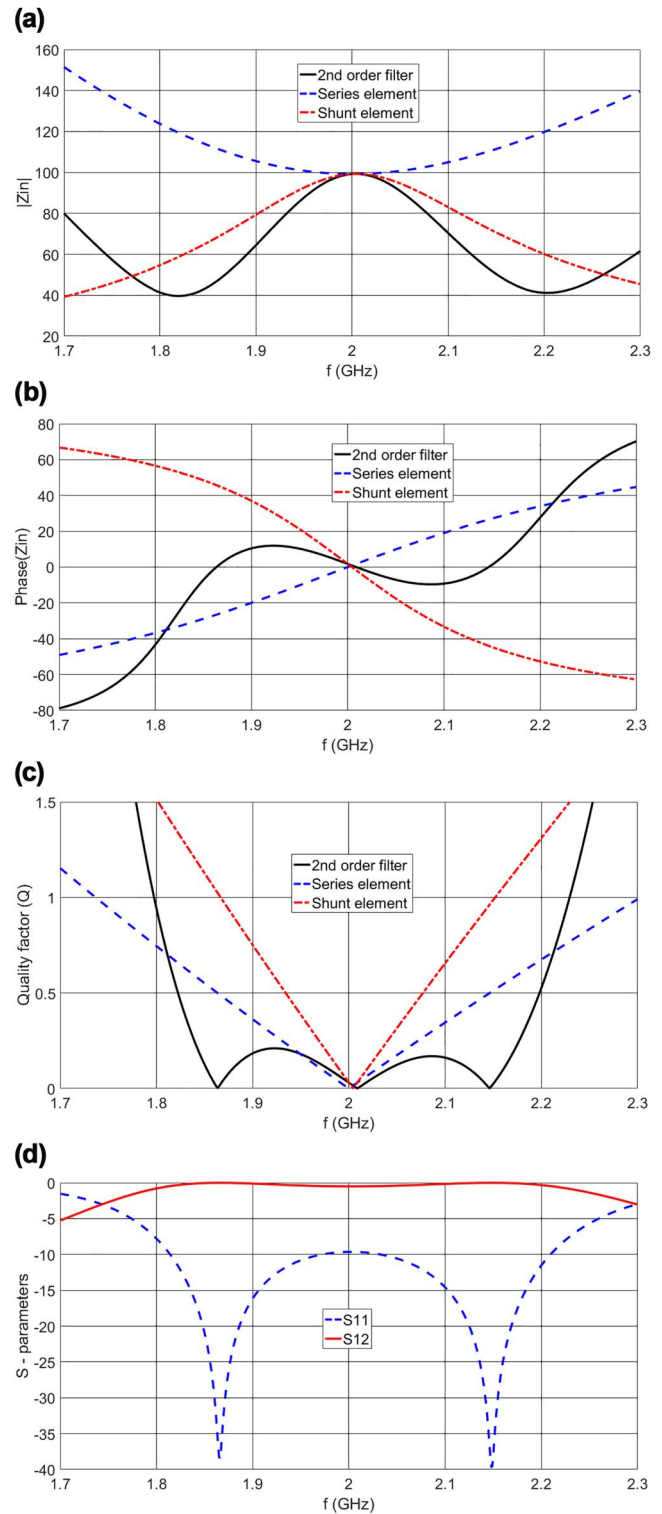**FIGURE 3** (a) Amplitude and (b) phase of input impedance. (c) Quality factor of the series and parallel resonator, each one alone and their combination as in the circuit of the band-pass filter (BPF) of Figure 2. (d) S-parameters of BPF

short-circuited or half wavelength open-circuited stubs, which behave as parallel resonant circuits. The classical BPF approach is based on using quarter wavelength stubs short-circuited to

TABLE 1 Voltage transfer function and resonant frequencies of band-pass filters for orders $n = 1, 2,$ and 3

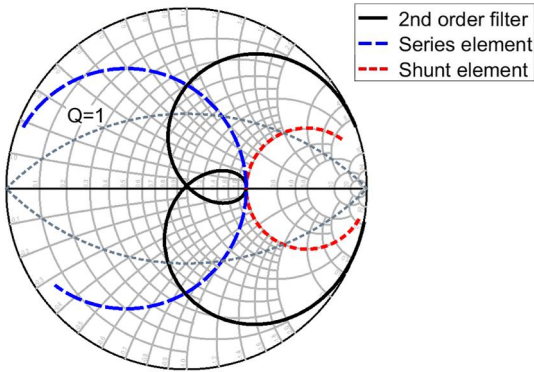| n	$H(j\omega)$	ω_r
1	$\dfrac{R_L}{R_L + Z_1}$	$\omega_0 = \dfrac{1}{\sqrt{L_1 C_1}}$
2	$\dfrac{R_L Z_2}{Z_1 Z_2 + R_L(Z_1 + Z_2)}$	$\omega_{1,2} = \omega_0 \left[\dfrac{2 + A\left(1 \pm \sqrt{1 + 4\frac{1}{A}}\right)}{2} \right]^{\frac{1}{2}}$ $A = \dfrac{L_2}{L_1}$
3	$\dfrac{R_1 Z_2}{Z_1 Z_2 + (R_L + Z_3)(Z_1 + Z_2)}$	$\omega_2 = \omega_o \omega_{1,3} = \omega_0 \left[\dfrac{2 + A\left(1 \pm \sqrt{1 + 4\frac{1}{A}}\right)}{2} \right]^{\frac{1}{2}}$ $A = \dfrac{L_2}{L_3} + \dfrac{L_2}{L_1}$

FIGURE 4 Impedance locus of a shunt resonance, a series resonance and the cascaded connection of them at $f_o = 2$ GHz

FIGURE 5 The equivalent circuit of a rectangular patch antenna resonating in the TM_{100} mode

the ground plane through metallised vias. On the contrary, herein, open circuited half wavelength stubs are utilised as patch antennas. For a chosen response, the prototype parameters g_n are given by standard tables. In the ordinary BPF, by matching the stubs and resonator input impedances, the stub characteristic impedance is calculated as [28]

$$Z_{0,n} = \pi Z_o \Delta / (4g_n) \tag{5}$$

where Δ is the fractional bandwidth and Z_o the characteristic impedance of the admittance inverter (Figure 1b).

These shunt stubs can be readily substituted by rectangular patch antennas to directly obtain a frequency pulled antenna.

However, the utilised printed antennas operate at their parallel resonance when their length is half wavelength and their edges are open-circuited. Hence, the BPF must be realised utilising open-circuited, half wavelength shunt stubs. In this case, the elements of the parallel equivalent circuit are estimated by extracting an approach similar to [28],

$$\left. \begin{array}{l} L_n = \dfrac{\Delta Z_0}{\omega_o g_n} = \dfrac{2 Z_{0,n}}{\pi \omega_o} \\[3mm] C_n = \dfrac{g_n}{\omega_o \Delta Z_0} = \dfrac{\pi}{2\omega_o Z_{0,n}} \end{array} \right\} \leftrightarrow Z_{0,n} = \dfrac{\pi \Delta Z_0}{2g_n} \tag{6}$$
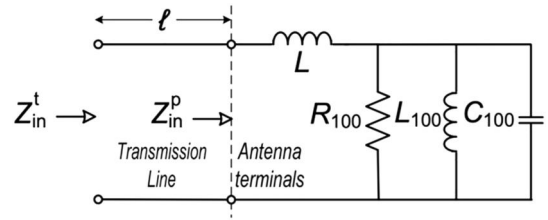
2.3 | Equivalent circuit of the patch antenna

For the successful substitution of half-wavelength open-circuited stubs with patch antenna elements, their equivalent electrical circuits must be identical. When a rectangular patch antenna (RPA) is operated within the bandwidth of one of its resonant modes (e.g. at TM_{100}), the corresponding parallel resonant circuit is dominant and its equivalent circuit is shown in Figure 5 [11, 29]. Although for the calculation of parallel resonance parameters, R, L, and C, for each individual mode, closed form expressions exist [28]; these can be also extracted from measurement or simulation results. Since the aim is to design arbitrary-shaped wideband antennas, we estimate these parameters from simulated input impedance results. We choose to use this method, since it is more accurate and general, and we use the expressions to verify the produced results. The RPA is designed following established procedures by simulation in IE3D™, a commercial method of moments code well suited for planar structures. Thus, for every different feeding point, the input impedance is obtained. In turn, its parallel equivalent circuit can be extracted following the same way as for the open half-wavelength stubs.

Following the well-known design procedure, we make the RPA to resonate at the desired central frequency $\omega_0 = 2\pi f_0$. The resistance R_p is estimated at the resonance, while the inductance and capacitance can be calculated from the impedance value at a frequency $\omega = \omega_o + \Delta\omega$ within the resonant mode bandwidth as shown in (2c):

$$R_{\rm p} = Z_{\rm in}(\omega = \omega_0) = Re\{Z_{\rm in}(\omega = \omega_0)\} \tag{7a}$$

$$C_{\rm p} = \frac{\omega}{\omega^2 - \omega_0^2} Im(Y_{\rm in}) \approx \frac{Im(Y_{\rm in})}{2\Delta\omega} \tag{7b}$$

$$L_{\rm p} = \frac{1}{\omega_0^2 C_{\rm p}} \tag{7c}$$

The subscript p denotes 'patch' and corresponds to the resonant mode, which here is the dominant mode TM_{100}. Alternatively, the reactive parameters can be calculated using the unloaded quality factor Q_0, which in turn can be estimated from the negative slope of the imaginary part of the impedance or from its phase according to Ref. [18] and the references cited therein, as

$$Q_0 = R_{\rm p}\omega_0 C_{\rm p} = R_{\rm p}/(\omega_0 L_{\rm p}) \tag{8a}$$

Then

$$C_0 = \frac{Q_0}{R_{\rm p}\omega_0} \tag{8b}$$

and

$$L_{\rm p} = \frac{R_{\rm p}}{Q_0\omega_0} \tag{8c}$$

$$Z_{\rm in}(\omega) = \left\{\frac{1}{R_{\rm p}} + j\omega C_{\rm p} + \frac{1}{j\omega L_{\rm p}}\right\}^{-1} \tag{8d}$$

$$Q_0 \approx -\frac{f_0}{2R_{\rm p}} Im\left\{\frac{\vartheta Z_{\rm in}(f)}{\vartheta f}\right\}\bigg|_{f=f_0} \tag{8e}$$

In general, for the calculation of the slope-derivative, a simulated or a measured $Z_{in}(\omega)$ can be used. Patch antennas are designed after choosing the operating frequency and a material for the dielectric substrate characterised by its thickness, dielectric constant and loss tangent [11]. The patch antenna can be inset-fed or probe-fed and when it operates at its dominant mode TM_{100}, it is replaced by its equivalent circuit as shown in Figure 5. The comparison of Figure 5 with the circuit of each resonator in Figure 1b shows that they are almost identical. The difference is the existence of the shunt resistor (radiation resistance), which has the role of the quality factor regulator of the antenna and the series inductance, which represents the feeding transmission line or probe where energy is stored corresponding to high order modes. Under matching conditions, the impedance $Z_{\rm in}^{\rm t}$ locus will be rotated on the Smith chart when the feeding line length is changed, but its matched operating frequency point will be retained at the centre. Hence the length in Figure 5 can be tuned to implement the desired resonators. The patch antenna feeding point, when either an inset or coaxial probe feed is utilised (Figure 5), is

selected for matching to the transmission line as $Re(Z_{\rm in}^{\rm p}) = Z_0$. The complex antenna input impedance as a function of frequency $Z_{in}^{p}(\omega)$ is herein estimated from electromagnetic simulation.

For a given central operating frequency ω_0, the antenna input impedance $Z_{\rm in}^{\rm t}(\omega)$, including the additional line as in Figure 5, should be made identical to the corresponding resonator of the filter $(L_{\rm p}, C_{\rm p})$ to be implemented. In turn $Z_{\rm in}^{\rm p}(\omega)$ is given by (8d), from the pth-stage $(L_{\rm p}, C_{\rm p})$ (Figure 2) and it can be equal to $Z_{\rm in}^{\rm p}(\omega)$ defined by Equation (2c). Hence, the feeding line length is estimated by the following expression:

$$Z_{\rm in}^{\rm t}(\omega) = Z_{\rm o}\frac{Z_{\rm in}^{\rm p}(\omega) + jZ_{\rm o}\tan(\beta l)}{Z_{\rm o} + jZ_{\rm in}^{\rm p}(\omega)\tan(\beta l)} \tag{9}$$

It is worth to be noted here that extra effort was paid to keep as central frequency the value of 2 GHz. The addition of feeding line length is equivalent to the addition of series inductance, which has as a result the rotation of the impedance on the Smith chart or shifting the bandwidth to higher frequency values. This is the reason that the FP bandwidth enhancement shown in prototypes of the next section is not centralised to the original central frequency but occurs around a higher frequency.

3 | ANTENNA DESIGN CASES

Although the main purpose of this work is the design of single compact wideband elements as option (i) described in the introduction, for clarification and convenience we start with the array of option (ii). This is a direct application of the band-pass filter approach explicitly designed in Section 2.2 and illustrated in Figure 1d. The only difference from the standard printed band-pass filter is the substitution of the short-circuited quarter wavelength stubs (typical BPF) by open-circuited half wavelength 'stubs', which are actually rectangular patch antennas. Notably, both of them behave as shunt parallel resonators.

Regarding the compact element design approach [option (i)], it follows the scheme of Figure 1e. Here, the same patch antenna is utilised to implement each resonator of the BPF topology through a different feeding point. The explicit implementation of option i and ii follows in the next subsections.

3.1 | Three and four elements array

The first case implements option ii defined in the introduction, namely to design a frequency-pulled array similar to the antenna array shown in Figure 1d. As was explained, the phase difference between adjacent patches is 90° (Figure 1b), and the dimensions of patches are calculated for the chosen operating frequency and dielectric substrate material. The input impedances of patches should be in agreement with the corresponding resonator of the related filter and are taken from Equation (9). By adjusting the

TABLE 2 Parameter dimensions of the 4 elements FP array (Figure 6), four-feed single patch (Figure 8) and multi-feed array (Figure 11), antennas

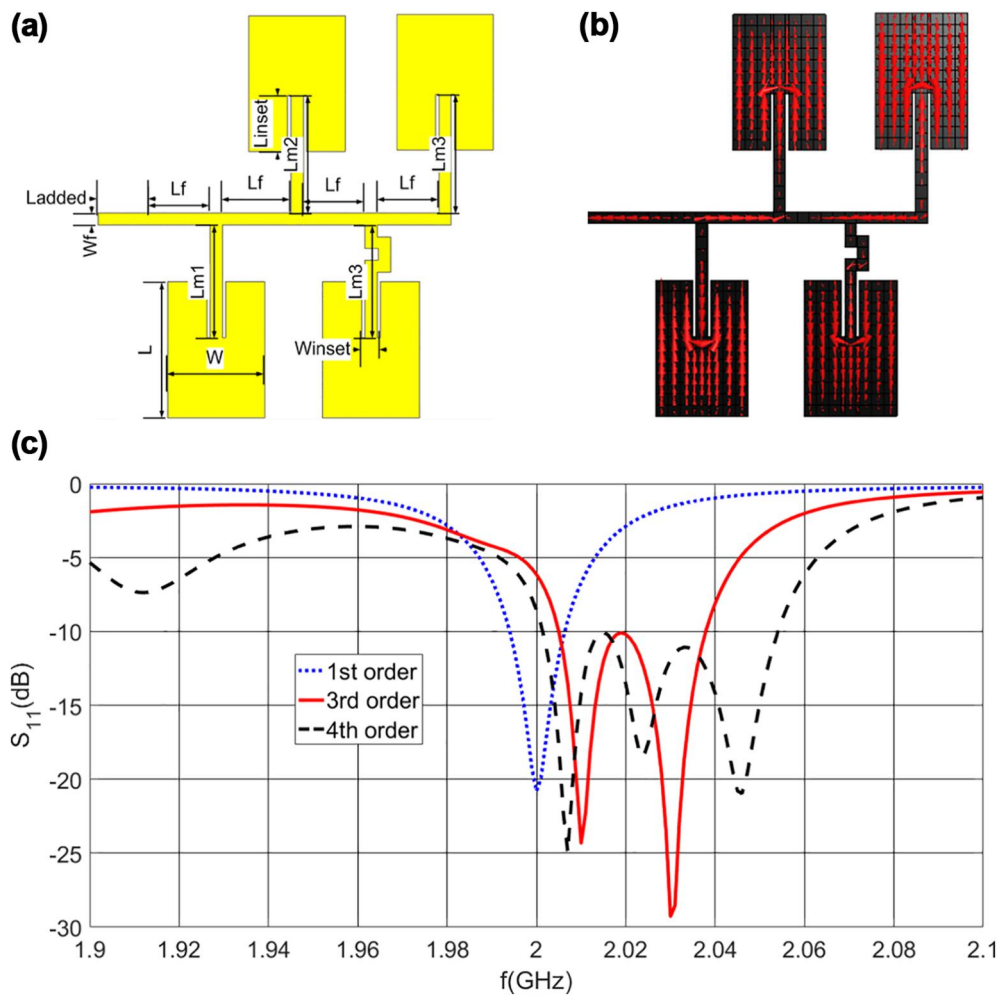| Parameter dimensions (mm)	Antenna of Figure 6	Parameter dimensions (mm)	Antenna of Figure 8	Parameter dimensions (mm)	Antenna of Figure 11a	Antenna of Figure 11b
L_f	20	L_g	46.48	L_g	128.79	183.04
W_f	3.56	W_g	46.48	W_g	60.98	67.98
L	41.25	L_p	30.99	d_1	39.80	39.80
W	28.2	x_f	3.87	d_2	19.26	29.26
L_{inset}	16.99	W_f	3.5	d_3	-	13.26
W_{inset}	5.5	L_1	30.79	L_1	44.25	44.25
L_{m1}	34.09	L_2	23.43	L_2	46.75	56.75
L_{m2}	35.68	L_3	8.93	L_3	-	40.75
L_{m3}	38.47	L_4	11.79	W_1	7	10.5
L_{m4}	36.09	L_5	11.25	W_2	3.5	11
		L_6	9.47	W_3	-	3.5
		L_7	11.25			
		L_8	20.11			

FIGURE 6 (a) Four elements FP antenna. (b) Current distribution at central frequency. (c) S_{11} of single element, and three and four-element array antennas

feeding line length, these values are seen at the connection point of every patch with the feeding line.

In order to show the bandwidth enhancement, two antenna arrays with three and four patches were designed corresponding to BPF of the third and fourth order, respectively, with centre frequency of 2 GHz. The values of all necessary parameters are given in Table 2. The antennas are shown (for space economy only one of the fourth order) along with their S_{11} parameters in Figure 6, where for comparison reasons, the case of a single patch antenna was also added. The elements are placed on alternate sides of the feeding line in order to obtain unidirectional and parallel current distributions (Figure 6b), which enhance the efficiency of the antenna. Patch elements are aligned parallel, using meander-feeding lines when it is necessary. In the proposed method, no load is needed because each antenna element has its own resistor (representing radiated power) in its equivalent circuit and so the only action needed is the tuning of the values of the equivalent circuit to the ones defined by the filter theory. This is realised through the different lengths of the feeding line of each element (Lm_1 to Lm_4). Although the last element does not radiate as much as the other elements, it is needed for the total band-pass behaviour. From Table 3 where the bandwidth edge frequencies for each antenna are given, the values of the total and fractional bandwidth can be calculated. These values are also shown in the same table, from which the bandwidth enhancement for the cases of three- and four-element array antennas can be estimated. It is obvious that the bandwidth

increases and it can be said that it is tripled and quadrupled, respectively, for the two cases of three- and four-element antennas with respect to a single-element antenna. For comparison reasons, the achieved fractional bandwidth of a typical eight elements array [30] was included, which although operating in different centre frequency presents roughly the same bandwidth in the case of the three elements array and smaller bandwidth than the case of the four elements array. In addition, the comparison with a four elements filtenna (third order BPF and antenna load) from Ref. [25] is shown, but it should be noted that in our case, the antenna elements have smaller W dimension and higher dielectric constant (ε_r = 3.5 instead of 2.2), which results in elements with narrower bandwidth.

Radiation patterns of the three- and four-element antennas are illustrated in Figure 7 for the three frequencies shown in Table 3. It is observed that as the number of elements increases, the main single lobe starts to split in two. Essentially, the expected beam squint or orientation towards 30° is observed in Figure 7 due to the −90° phase difference induced by the impedance inverters between successive elements. This renders the proposed FP inappropriate for arrays with strict desired radiation patterns. However, it is proved in the next section that FP is best suited for bandwidth enhancement of single elements exhibiting multiple symmetrical feeding points. These can in turn be utilised within classical array design without any restrictions and yield a radiation pattern free from any beam squint. This feature is explicitly proved in the wideband array design of Section 3.3.

(*number*) of elements	f_L (GHz)	f_C (GHz)	f_H (GHz)	BW (MHz)	Fractional BW (%)
1	1.995	2.002	2.009	14.02	0.70
3	2.008	2.026	2.043	34.87	1.72
4	2.003	2.031	2.058	54.49	2.68
8 [30]	27.9	28.15	28.4	500	1.776
4 [25]	4.925	5.0	5.075	150	3.0

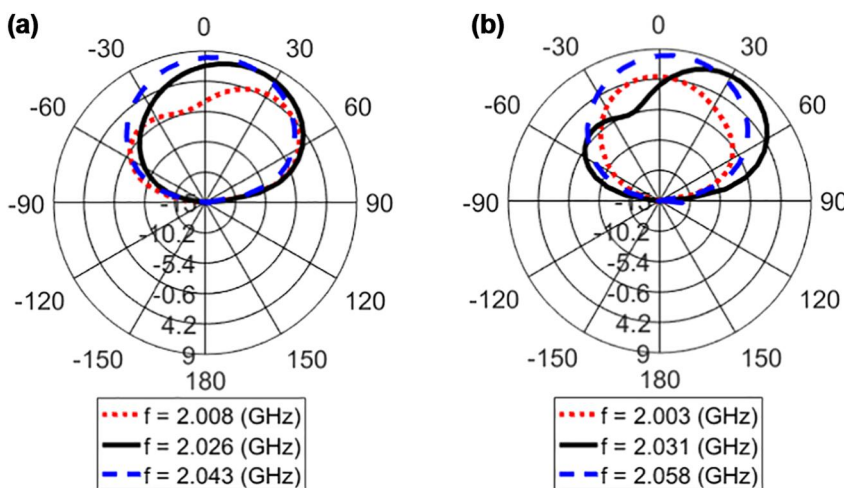**TABLE 3** Bandwidth frequencies for the antennas of Figure 6.

FIGURE 7 Radiation patterns of three- and four-element antennas for frequencies of Table 3. Elevation plane for three elements (a) and four elements (b) antennas

3.2 | Compact single-element antenna

The second design elaborates on option (i) defined in the introduction, namely the single-compact element with multiple symmetrical feeding points. The different resonators required by FP can be offered by a single physical radiating element (e.g. Figure 8a) when it exhibits multiple symmetrical feeding points. A separate resonator is viewed at each corresponding input port, but all of them resonate at the same frequency (exciting the same mode). These exhibit identical resonant circuits (Z_{in}^p in Figure 5) apart from the transmission line utilised in Figure 5 to match each resonator with the corresponding BPF element.

Our first attempts applying FP to a rectangular and super-shaped patch antennas with two symmetrical feeding points are presented in Refs. [14–16]. Aiming at maintaining the antenna dimensions to minimum, a second dielectric substrate can be used, sharing the same ground plane with the first. The patch will be located on the top layer, while the feeding network will be printed on the bottom layer. The feeding is achieved with metallised vias by connecting each feeding point with the feeding network. For the implementation, the antenna and the feeding network will be printed on separate substrates. These will then be placed back-to-back and their ground planes will be glued or soldered together.

A variety of patch antenna shapes exhibit symmetrical feeding points and FP can be applied to any one of those. Among them the canonically shaped patch radiators—equilateral triangle, square and canonical N-agon—pentagon, hexagon, heptagon etc. are of particular interest due to their high degree of symmetry. Although we plan to study most of them, herein, we focus on square–tetragonal for convenience reasons.

In order to test the FP technique for greater bandwidth enhancement, instead of a rectangular, a square patch is selected, which has four symmetrical feeding points. Using two, three or four of them, the antennas equivalent to the second, third or fourth order filter can be produced, respectively. The feeding line length is selected to achieve the appropriate equivalent circuit and to induce the −90° phase difference needed for the impedance inverters. It is important to mention that the FP technique can be used with different shape radiators, such as super shapes, resulting to a much wider bandwidth [15].

A square patch antenna with four symmetrical feeding points, designed as a fourth order BPF, is shown in Figure 8. Its design parameter values are given in Table 2, and the resulting bandwidth frequencies, total and fractional bandwidths are given in Table 4. In Figure 8d the reflection coefficient is shown, where for comparison reasons the cases of the first to third order BPF were added. The ideal tuning of each resonance's L and C would result in the right number of resonances (aka four), but this is difficult with all the elements being fed by the same line. This is the reason we are focussing on bandwidth enhancement as the fractional bandwidth and not on the number of resonances.

For a better comprehension, in Figure 8e a parametric analysis for some key dimensions of the antenna of Figure 8 is
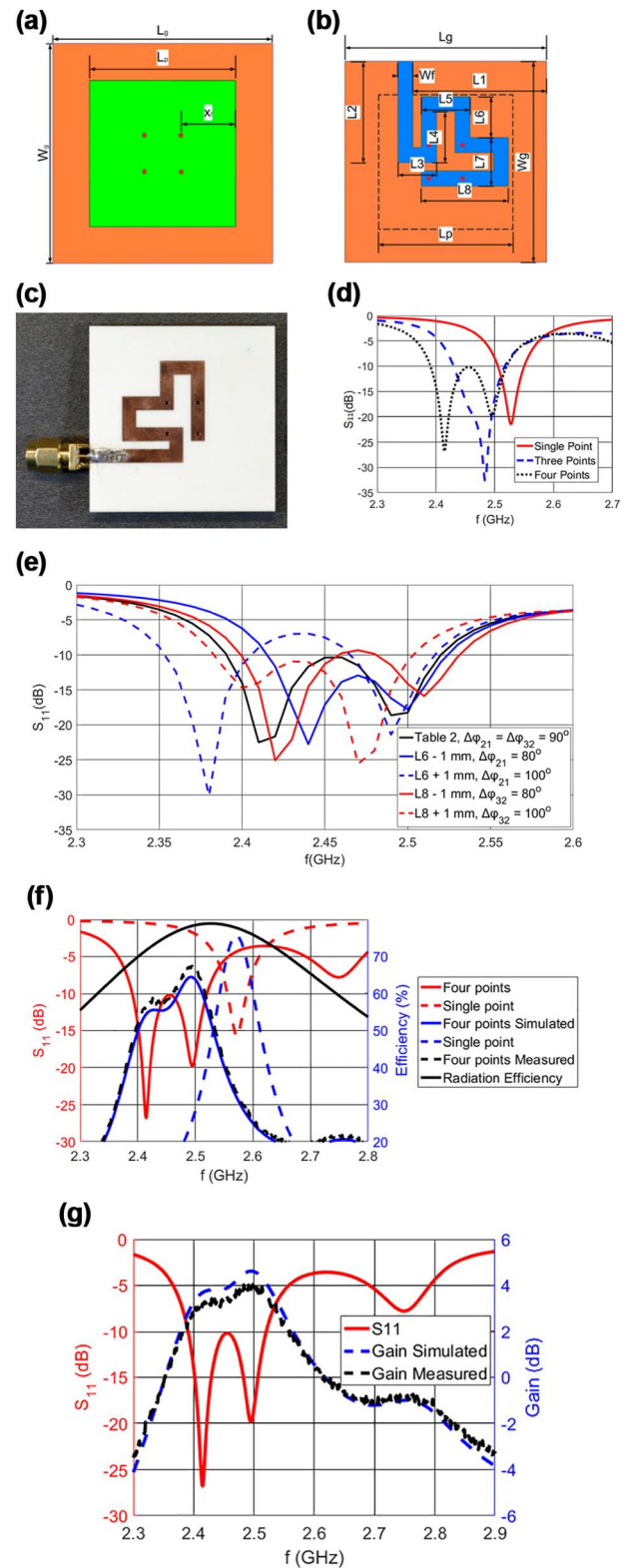

FIGURE 8 Square patch antenna with four symmetrical feeding points: (a) top view, (b) feeding network for the fourth order filter antenna with dimensions given in Table 2, (c) fabricated prototype and (d) reflection coefficient of multiple feeding point antennas (first, third and fourth order filter), (e) reflection coefficient of the four feeding point antenna parametric analysis (Δφ indexes represent the feeding points starting from the closest to the feeding port) (f) efficiency and (g) gain for the fourth order filter antenna

(Number) of elements	f_L (GHz)	f_C (GHz)	f_H (GHz)	BW (MHz)	Fractional BW (%)
1	2.552	2.568	2.583	31	1.2
3	2.43	2.474	2.517	87	3.52
4	2.39	2.455	2.52	130	5.3

TABLE 4 Bandwidth frequencies for the multi-feed square patch antenna of Figure 8.
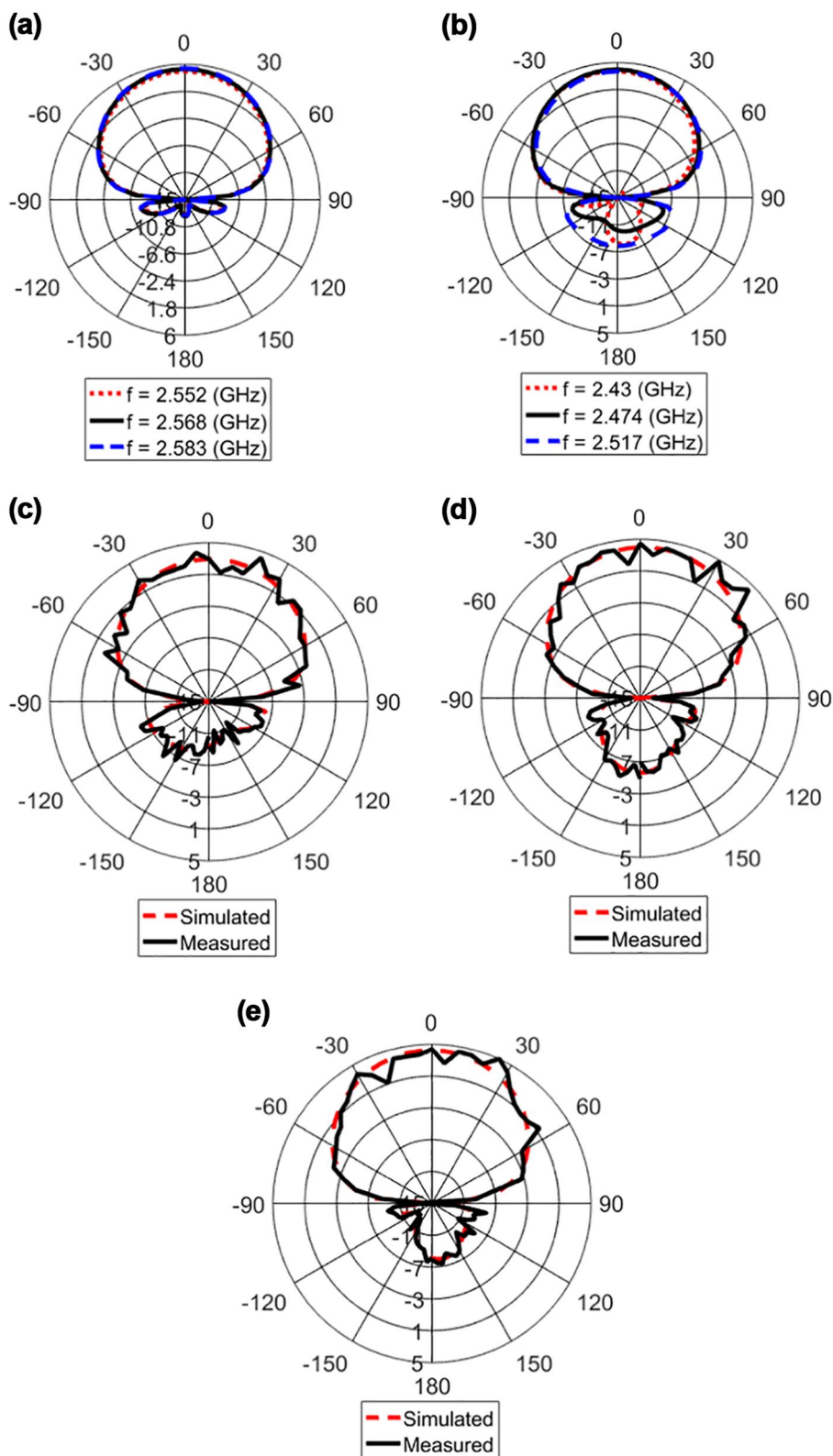

FIGURE 9 Radiation patterns of the multi-feed square patch antenna for frequencies of Table 3. The elevation plane for (a) single feeding, (b) third order, simulated and measured, (c) fourth order filter at 2.39 GHz, (d) fourth order filter at 2.455 GHz and (e) fourth order filter at 2.52 GHz antennas

FIGURE 10 Simulations and measurement results for the square patch antenna with four symmetrical feeding points
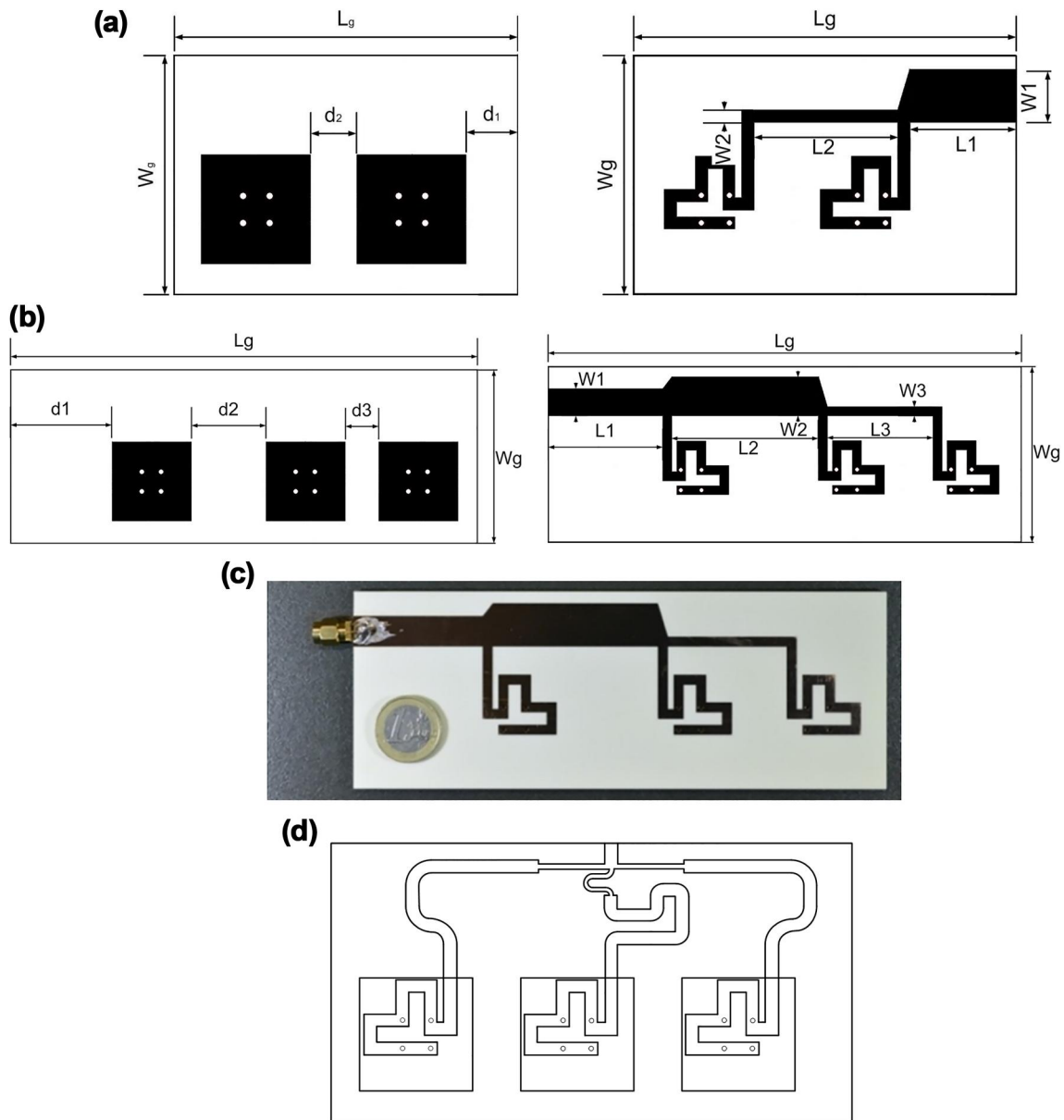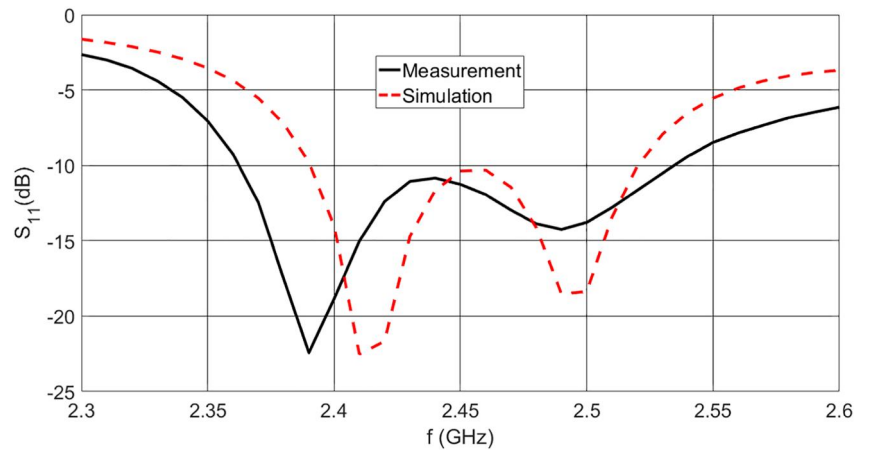

FIGURE 11 Wideband travelling wave multi-feed antenna. (a) Top and bottom (feeding network) view for the two elements array, (b) top and bottom (feeding network) view for the three elements array, (c) manufactured prototype for measurements and (d) array with in phase multi-fed compact elements

shown. The purpose of the analysis is the examination of how the shift in resonances affects the impedance matching and in turn the bandwidth. Since this is controlled by the admittance inverters between successive resonators, the corresponding electrical lengths are perturbed above and below −90°. Explicitly the increasing or decreasing of dimensions L6 or L8, affects the phase difference between consecutive feeding points. Specifically, adding 1 mm to the length of the line between two feeding points increases the phase difference almost by 10° (10.9°) while reducing the same length by 1 mm decreases the phase difference by almost 10° as well. The length between the feeding points 3 and 4 has not been studied because the optimum response has been achieved for it to be minimum (straight line with no turns) and as such it is not possible to be further decreased. However, theoretically, the same principle as with the two other lengths can be followed. The resulting reflection coefficient (S_{11}) illustrated in Figure 8e shows that the variation of phase difference by L6, and L8 causes shifts in the resonances. As expected, pulling successive resonances too far apart (L6 + 1 mm, $\Delta\varphi = -100°$, the first resonance shift to 2.38 GHz from 2.415 GHz) causes an increase in S_{11} above the limit of −10 dB. The optimal bandwidth is obtained when the ideal −90° phase shift is attained, just as predicted theoretically.

The radiation patterns for the frequencies of Table 4 are presented in Figure 9. It is observed that the same radiation pattern is retained across the whole operating bandwidth, while the deformation of the main lobe that happened for the antenna array of the same order of Figure 7 does not occur here. As explained before, the reason for the main lobe splitting and the beam squint is caused by the −90° phase difference between elements due to the impedance inverters between successive elements. However, in the compact square patch two modes (TM_{100} and TM_{010}) are simultaneously excited by the corresponding pairs of feeding points in the square patch of Figure 8 and the −90° phase difference simply results to a circularly polarised radiation pattern. Notably, for a rectangular patch operating at a single (e.g. the dominant) mode frequency pulling through the two symmetrical feeding points retains the linear polarisation [13]. In Figure 9, the back lobe is a result of the feeding network in the back side of the antenna (second substrate), which in the worst-case scenario (Figure 9d) is below −10 dB compared to the main lobe maximum. The improved radiation pattern and the fact that this antenna presents more than double the bandwidth of the multiple elemental previous one, proves that this case is a better design. Figure 10 presents a comparison between simulation and measurement results from a manufactured prototype.

3.3 | Three compact wideband elements FP array

Frequency pulling according to the third (iii) option as identified in the introduction is attempted in this design. For this purpose, the FP approach is used two times or in two levels: an FP antenna array is designed using appropriate impedance lines but with the patch antenna elements replaced by the multi-feed compact (Section 3.2) square elements equivalent to fourth order filters. The multi-feed shifts the frequency downwards while the use of multiple elements causes upward shifts. As a result, an extended bandwidth is produced. The resulting array is illustrated in Figure 11 (a, for two elements and b, for three
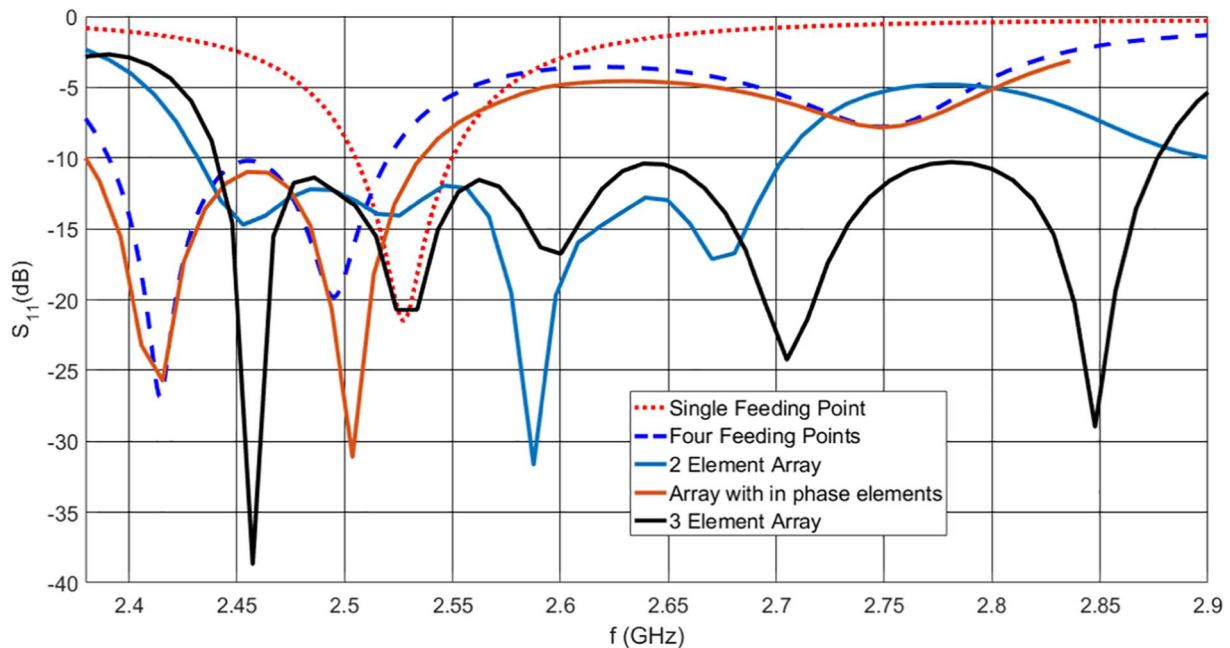

F I G U R E 1 2 Reflection coefficients for the antennas of Figures 6, 8 and 11

elements), and its design parameter values are given in Table 2 while the corresponding reflection coefficient, compared to those of previous design stages is presented in Figure 12. Comparing Figure 6 with Figure 11, the design approach is actually the same. In both cases, we have an array consisting of 4 and 3 elements, respectively. The only difference is that in Figure 6 the elements used are planar antennas with a single substrate and as such of narrow bandwidth, while in Figure 11 as an element we use the antenna of Figure 8, which offers greater bandwidth. So, it is only an issue of matching for narrow band and wider band elements. This is the reason for the different dimensions of lines (d_1, d_2, d_3, W_1, W_2, and W_3), resulting in the uncommon array shape between the elements

in order to achieve proper matching (L and C for each element). Utilising three compact multi-feed array antennas, it is expected to have a bandwidth increase by about three times in respect to that of Table 4. This yields an overall increase of around 12 times in bandwidth compared to the ordinary square patch antenna fed in a single point. Finally, a comparison of important frequencies and efficiencies (maximum values) is carried out as depicted in Table 5 for two and three compact elements arrays. The initial bandwidth increase expectation is achieved. The radiation pattern of the array is presented in Figure 13 and a comparison between the measurements of the fabricated prototype and simulations results is shown in Figure 14.

T A B L E 5 Bandwidth frequencies and efficiencies for single, four-feed square patch and multi-feed array antennas

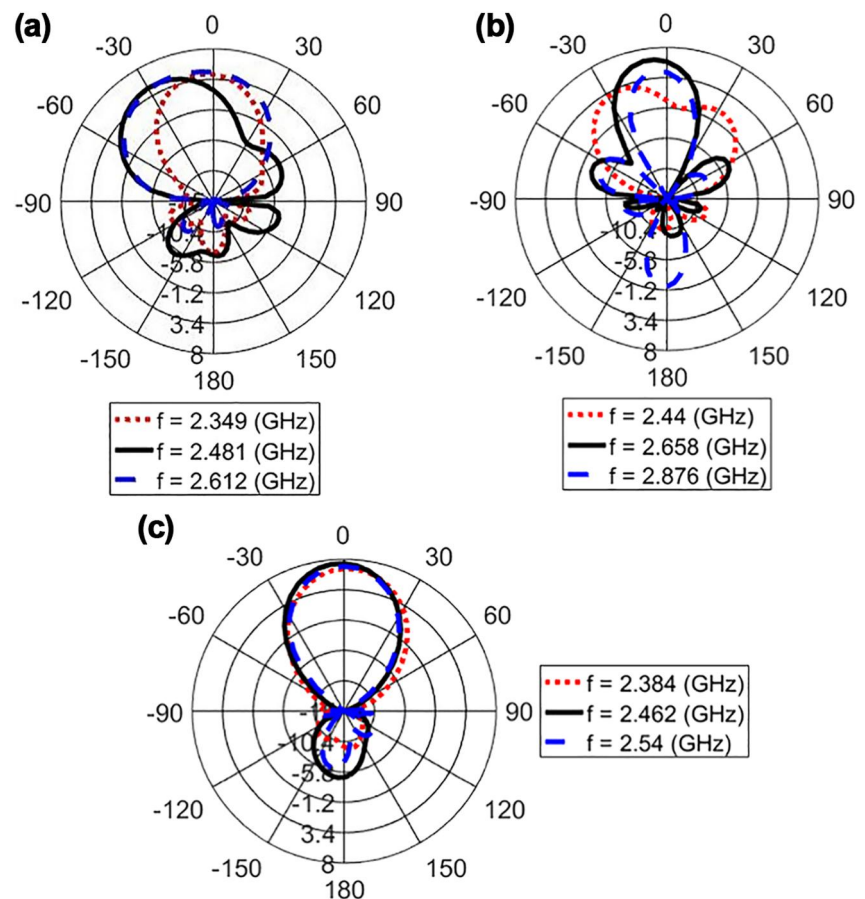|	Single feed patch	Square 4 -point feed patch (Figure 8)	Two element array antenna (Figure 11a)	Three element array antenna (Figure 11b)
f_L (GHz)	2.552	2.39	2.349	2.44
f_C (GHz)	2.568	2.455	2.481	2.658
f_H (GHz)	2.583	2.52	2.612	2.876
Peak antenna efficiency (%)	73.1	64.36	62.1	59.9
BW (MHz)	31	130	263	436
BW (%)	1.2	5.3	10.6	16.4

FIGURE 13 Elevation radiation patterns for frequencies of Table 5 of multi-feed array antennas comprised of (a) two elements, (b) three elements and (c) array with in phase multi-fed compact elements
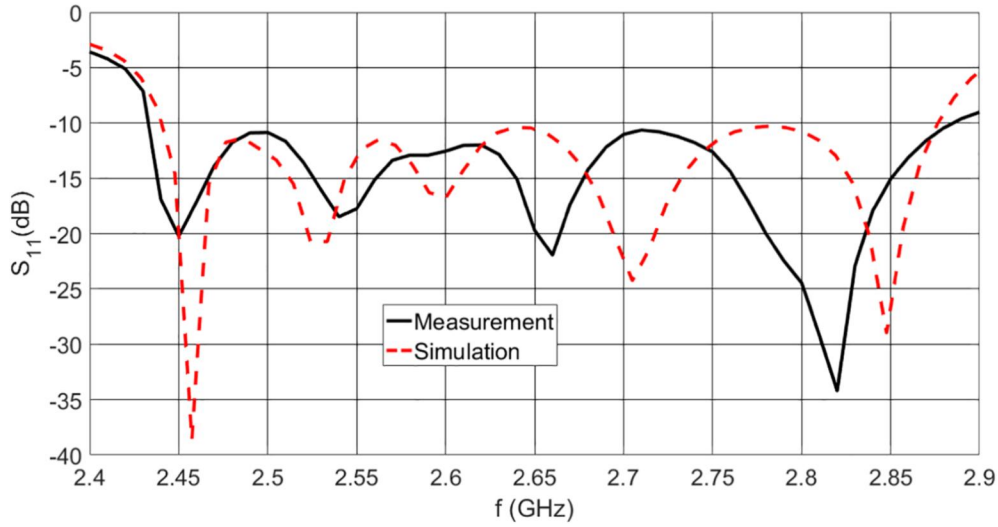
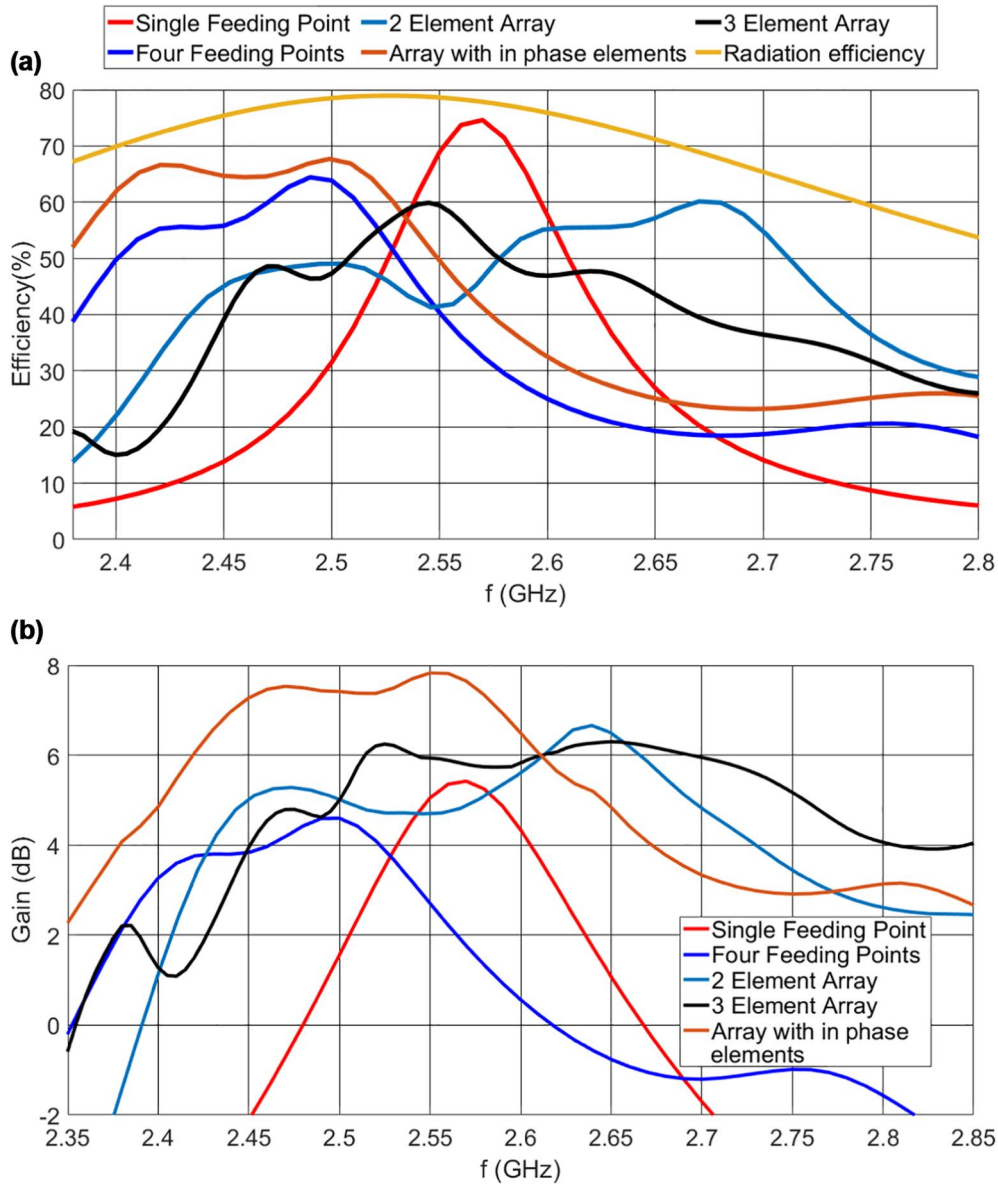**FIGURE 14** Simulation and measurement results for the multi-feed array antenna

FIGURE 15 Radiation characteristics of antennas compared in Figure 12. (a) Efficiency versus frequency. (b) Gain versus frequency

3.4 | Classical array of three compact elements

The beam squint or orientation towards 30° occurred in the two arrays of Figures 7 and 13a, b is attributed to the phase difference of −90° between elements inserted by the corresponding impedance inverters. In order to prove this reasoning but also to demonstrate that the frequency pulled multi-point fed compact elements (e.g. Figure 8 and Section 3.2) can be exploited within classical array design, such an array is elaborated in Figure 11d.

The basic difference from the other two arrays is that no attempt is made to apply a second order FP and for simplicity, the feeding network is designed to provide equal phases to the three elements of Figure 11d. Indeed, a broadside radiation pattern is observed in Figure 13c free from any beam squint. However, as expected the impedance bandwidth of this array is retained almost identical (slightly widened) to that of the utilised 4-point feed compact element as shown in Figure 12. Thus, when aiming at arrays, the bandwidth enhancement effort should be directed only towards the multipoint-fed frequency-pulled elements. Towards this direction, a combination of FP with inherent multiple resonance elements (i.e. square patches with truncated corners and/or etched diagonal slots) will be sought in our next task.

3.5 | Performance in efficiency and gain

All elaborated structures are compared in Figure 15 in terms of efficiency and gain. Regarding the antenna efficiency, a type of 'Fano's gain limit' is observed in Figure 15a with reference to the ideal element radiation efficiency. Explicitly, the antenna efficiency of the single feeding point patch is higher (73%)

approaching the radiation efficiency value (78%) but with the narrowest bandwidth. As the bandwidth is increased by FP, the maximum antenna efficiency remains lower than the radiation efficiency at any frequency across the operating band. For this reason, the three elements in the phase array have an antenna efficiency of 62% close to that of its single quad-fed element, while the maximum value for the three element FP array drops to about 60%.

Regarding the gain of Figure 15b, it is relatively following the antenna efficiency with some alteration caused by the additional loss introduced by the feeding network. As expected, the arrays have a higher gain due to the increased directivity. The classical design of the three compact elements broadside array shows the highest gain and verifies the expectation of exploiting these elements in standard array design.

3.6 | Discussion and comparisons

The characteristics of the proposed single compact element antenna and the proposed arrays are compared with the corresponding one in the literature in Tables 6 and 7. With regard to the single element (Table 6), the proposed antenna is more compact (small size) and has higher gain. Besides that the competitive antennas [22, 24, 26] share essentially the same principle as the FP herein to enhance the impedance bandwidth. Namely, they place a band-pass filter at the input port of the antenna aiming at the compensation of the reactive part of the antenna input impedance. Instead, the proposed technique formulates the patch antenna as a band-pass filter by utilising each one of its symmetric feeding points as a resonator. These work are actually following the impedance broad-banding techniques proposed by Fano [31]

TABLE 6 Comparison of the compact proposed single element antenna with the corresponding in the literature (PG stands for peak gain)

Reference	Size	f_c (GHz)	BW (%)	PG (dBi)
[22][a]	$0.41\lambda_o \times 0.6\lambda_o \times 0.01\lambda_o$	2.45	14	2.53
[23][a]	$0.79\lambda_o \times 0.59\lambda_o \times 0.025\lambda_o$	2.4	8.3	2.3
[24]	$0.87\lambda_o \times 0.58\lambda_o \times 0.046\lambda_o$	4.16	4.7	4.3
[26][a]	$1.25\lambda_o \times 1.25\lambda_o \times 0.013\lambda_o$	2.45	8	4.6
Proposed antenna of Figure 8c	$0.47\lambda_o \times 0.47\lambda_o \times 0.025\lambda_o$	2.455	5.34	4.7

[a]Bidirectional patterns.

TABLE 7 Comparison of the proposed array antenna with the literature (NE, the number of elements and PG, the peak gain)

Reference	Size	f_c (GHz)	BW (%)	NE	PG (dBi)
[18]	$1.2\lambda_o \times 0.49\lambda_o$	2.485	14.9	4	4.73
[19]	$0.93\lambda_o \times 0.63\lambda_o$	2	3.64	3	20.32
[30]	$5.19\lambda_o \times 0.48\lambda_o$	28.15	1.776	8	24.4
[25]	$1.23\lambda_o \times 1.29\lambda_o$	5	3	4	9.6
Proposed array of Figure 11c	$3.05\lambda_o \times 1.28\lambda_o$	2.658	16.4	3	6.23
Proposed array of Figure 11d	$2.11\lambda_o \times 1.21\lambda_o$	2.513	6.3	3	7.82

and latter clarified by Youla in Ref. [32] who exactly suggested the introduction of a filter at the antenna input port to achieve broad banding. On this basis, the proposed technique goes a step forward by implementing Fano's and Youla's filter utilising the patch antenna symmetric feeding ports themselves. Referring to the cases [22, 23, 26], noted by a star superscript in Table 6, they are essentially monopole antennas with a bidirectional radiation pattern, which is reflected to a lower gain of about 2 dBi.

Discussing the array of 3 compact elements (Figure 11c) indeed offers the largest bandwidth as compared with the corresponding one in the literature. However, regarding the achieved gain this is lower, since there was not any effort towards beamforming, which was sacrificed to increase the bandwidth. As explained before, applying the FP at a second level (array level) indeed compromises the radiation pattern causing the beam squint. Hence, the second level FP is abandoned and the resulting wideband compact elements (Figure 8) are indicatively utilised in a classical array (Figure 11d) also depicted in Table 7. Indeed this delivers the expected gain of 7.82 dBi for a three element array but its bandwidth is retained at the same level (1% higher) as that of the single element.

4 | CONCLUSIONS

The FP technique for design compact patch antennas with extended bandwidth has been presented and characteristic design cases were shown. The multi-feed single patch approach gives bandwidth enhancement but with the size of a single patch. The choice of more feeding points using different patch shapes can further increase the bandwidth. The combination of the travelling wave antenna with multi-feed radiators indeed yields significant bandwidth enhancement but at the expense of the beam squint due to the $-90°$ phase difference induced by impedance inverters. It is of primary importance that the obtained wideband compact elements can be utilised within the standard array design but only with their inherent circular polarisation. For linear polarisation, compact elements as rectangular patches with two symmetrical feeding points can be utilised as polarisation is retained through FP. The detailed analysis of these limitations and the exploitation of single elements with inherent multiple resonances (truncated corners or slotted patches) will be the subject of future work.

CONFLICT OF INTEREST
The authors declare they have no conflict of interest.

DATA AVAILABILITY STATEMENT
Data available on request from the authors.

ORCID
Anastasios G. Koutinos https://orcid.org/0000-0002-8050-0085
George A. Kyriacou https://orcid.org/0000-0001-5253-0896
John L. Volakis https://orcid.org/0000-0002-0115-2079
Michael T. Chryssomallis https://orcid.org/0000-0002-3319-0096

REFERENCES

1. Volakis, J., Chen, C., Fujimoto, K.: Small Antennas: Miniaturization Techniques and Applications, ISBN-13: 978-0071625531. McGraw-Hill, New York (2010)
2. Tawk, Y., et al.: Antenna Design for Cognitive Radio. ISBN-13: 978-1608079537. ArtechHouse, Norwood (2016)
3. Cheng, J.-C., Dib, N.I., Katehi, L.P.B.: Theoretical modeling of cavity-backed patch antennas using a hybrid technique. IEEE Trans. Antennas Propag. 43(9), 1003–1013 (1995). https://doi.org/10.1109/8.410218
4. Huynh, T., Lee, K.-F.: Single-layer single-patch wideband microstrip antenna. Electron. Lett. 31(16), 1310–1312 (1995). https://doi.org/10.1049/el:19950950
5. Sanad, M.: Double C-patch antennas having different aperture shapes. In: IEEE APS International Symposium, Newport Beach, CA, USA, pp. 2116–2119 (1995). https://doi.org/10.1109/APS.1995.531012
6. Xiao, S., et al.: Bandwidth enhancing ultralow-profile compact patch antenna. IEEE Trans. Antennas Propag. 53(11), 3443–3447 (2005). https://doi.org/10.1109/tap.2005.858838
7. Chen, Y., Yang, S., Nie, Z.: Bandwidth enhancement method for low profile e-shaped microstrip patch antennas. IEEE Trans. Antennas Propag. 58(7), 2442–2447 (2010). https://doi.org/10.1109/tap.2010.2048850
8. Chair, R., Lee, K., Luk, K.: Bandwidth and cross-polarization characteristics of quarter-wave shorted patch antennas. Microw. Opt. Technol. Lett. 22(2), 101–103 (1999)
9. Waterhouse, R.: Microstrip patch antennas. In: Godara, L. (ed.) Handbook of Antennas in Wireless Communications, ISBN-13: 978-0849301247. CRC Press, London (2001)
10. Kala, P., Pant, R.: L-probe fed planar-rectangular microstrip patch antenna mounted on a cylindrical ground surface. Int. J. Microw. Opt. Tech. 5(2), 58–65 (2010)
11. Balanis, C.: Microstrip and mobile communications antennas. Antenna Theory Analysis and Design, 3rd ed., pp. 811–882. Wiley, London (2005)
12. James, J., Hall, P.: Handbook of Microstrip Antennas, 2nd ed., pp. 415–469. IET, London (1989)
13. Koutinos, A., et al.: A two-element patch antenna exploiting path inequality for bandwidth augmentation. In: 9th European Conference on Antennas and Propagation, Portugal, Lisbon pp. 1–5 (2015). https://ieeexplore.ieee.org/document/7228861
14. Koutinos, A., et al.: A wideband matching technique for polarization versatile applications. In: Progress in Electromagnetics Research Symposium, Prague, Czech Republic, pp. 2081–2086 (2015)
15. Koutinos, A., et al.: Bandwidth enhancement of a supershape patch antenna using multiple feeding technique. In: International Workshop on Antenna Technology: Small Antennas, Innovative Structures and Applications, Athens, Greece, pp. 211–214 (2017). https://doi.org/10.1109/IWAT.2017.7915360
16. Koutinos, A., et al.: Novel quadruple-fed rectangular patch antenna with improved bandwidth performance. In: IEEE 11th Loughborough Antennas & Propagation Conference, pp. 1–5 (2015)
17. Roh, W., et al.: Millimeter-wave beamforming as an enabling technology for 5G cellular communications: theoretical feasibility and prototype results. IEEE Commun. Mag. 52(2), 106–113 (2014). https://doi.org/10.1109/mcom.2014.6736750
18. Ludlow, P., et al.: Applying band-pass filter techniques to the design of small-aperture evanescent-mode waveguide antennas. IEEE Trans.

Antennas Propag. 61(1), 134–142 (2013). https://doi.org/10.1109/tap.2012.2220314

19. Mahmud, R.H., Lancaster, M.J.: High-gain and wide-bandwidth filtering planar antenna array-based solely on resonators. IEEE Trans. Antennas Propag. 65(5), 2367–2375 (2017). https://doi.org/10.1109/tap.2017.2670443

20. Yusuf, Y., Gong, X.: Compact low-loss integration of high-Q 3-D filters with highly efficient antennas. IEEE Trans. Microw. Theory Tech. 59(4), 857–865 (2011). https://doi.org/10.1109/tmtt.2010.2100407

21. Chen, F., et al.: X-band waveguide filtering antenna array with nonuniform feed structure. IEEE Trans. Microw. Theory Tech. 65(12), 4843–4850 (2017). https://doi.org/10.1109/tmtt.2017.2705697

22. Wu, W., et al.: A new compact filter-antenna for modern wireless communication systems. IEEE Antennas Wirel. Propag. Lett. 10, 1131–1134 (2011). https://doi.org/10.1109/lawp.2011.2171469

23. Chen, X.-W., et al.: A compact filtering antenna with flat gain response within the passband. IEEE Antennas Wirel. Propag. Lett. 12, 857–860 (2013). https://doi.org/10.1109/lawp.2013.2271972

24. Zuo, J., et al.: An integrated approach to RF antenna-filter co-design. IEEE Antennas Wirel. Propag. Lett. 8, 141–144 (2009). https://doi.org/10.1109/lawp.2009.2012732

25. Lin, C.-K., Chung, S.J.: A filtering microstrip antenna array. IEEE Trans. Microw. Theory Tech. 59(11), 2856–2863 (2011). https://doi.org/10.1109/tmtt.2011.2160986

26. Ohira, M., Ma, Z.: An efficient design method of microstrip filtering antenna suitable for circuit synthesis theory of microwave bandpass filters. In: International Symposium on Antennas and Propagation, Hobart, TAS, Australia, pp. 1–4 (2015). https://ieeexplore.ieee.org/document/7447517

27. Doane, J.P., Sertel, K., Volakis, J.L.: A wideband, wide scanning tightly coupled dipole array with integrated balun (TCDA-IB). IEEE Trans. Antennas Propag. 61(9), 4538–4548 (2013). https://doi.org/10.1109/tap.2013.2267199

28. Pozar, D.: Microwave Engineering, 4th ed., pp. 380–450. Wiley, London (2011)

29. Ansarizadeh, M., Ghorbani, A., Abd-Alhameed, R.A.: An approach to equivalent circuit modeling of rectangular microstrip antennas. Progress Electromagn. Res. B 8, 77–86 (2008). https://doi.org/10.2528/pierb08050403

30. Ishfaq, M., et al.: 8 × 8 Phased series fed patch antenna array at 28 GHz for 5G mobile base station antennas. In: IEEE-APS Topical Conference on Antennas and Propagation in Wireless Communications (APWC), Verona, Italy, pp. 160–162 (2017). https://doi.org/10.1109/APWC.2017.8062268

31. Fano, R.: Theoretical limitations on the broadbanding of arbitrary impedances. J. Frankl. Inst. 249(1), 57–83 (1950)

32. Youla, D.: A new theory of broad-band matching. IEEE Trans. Circuit Theory. 11(1), 30–50 (1964). https://doi.org/10.1109/tct.1964.1082267